FLOW STRUCTURE IN CORE CATCHER COOLING LOOP THROUGH AN INCLINED-TO-VERTICAL ELBOW BEND

K. W. Song, N. T. Hung, H. S. Park, and Shripad T. Revankar*
Division of Advanced Nuclear Engineering, POSTECH
Pohang, Republic of Korea
k1song@postech.ac.kr; nthung@postech.ac.kr; hejsunny@postech.ac.kr; shripad@purdue.edu

B. W. Rhee, K. S. Ha, R. J. Park, and J. H. Song
Korea Atomic Energy Research Institute (KAERI)
Daejeon, Republic of Korea
bwrhee@kaeri.re.kr; tomo@kaeri.re.kr; rjpark@kaeri.re.kr; dosa@kaeri.re.kr

ABSTRACT

Core catcher system is considered in EU-APR1400 as a cooling method during severe accident. Understanding of two-phase flow structure in the core catcher loop is necessary to properly design the natural circulation cooling system. Therefore, measurement of void fraction distribution, profile and averaged value are carried out using conductivity probes at various key locations along the channel. Void fraction distribution along the channel undergoes a sudden change at the inclined to vertical elbow band. High speed camera view shows a flow regime transition in terms of a sudden change of two-phase flow characteristics which is caused by the bubble breakup at the elbow bend. Observing void fraction profile, voids are relatively evenly dispersed from top wall to bottom wall at the vertical channel after elbow bend. Center line averaged void fractions are obtained by integrating the local void fraction at various depth of center of channel. These data are essential to understand two-phase flow behavior in the core catcher loop. In addition, the database is suitable for system code development and validation in terms of void fraction distribution and flow pattern along the large channel.

KEYWORDS
Two-phase flow, Void fraction, Bubble breakup, Flow transition

1. INTRODUCTION

Two-phase natural circulation cooling methods have been used in nuclear power plants especially in advanced reactors to increase reliability of the cooling system. They employ thermal induced density differences of working fluids to generate natural circulation without any external power. Natural circulation is used to cool the core catcher system which is considered as countermeasures for core melting and vessel failure scenarios during severe accident. It is a passively actuating device, which arrests and retains the corium, and removes decay heat of discharged molten core from reactor vessel by circulating water supplied from IRWST (In-containment Recirculation Water Storage Tank). Final goal of the system is to cool and stabilize corium inside the reactor cavity without MCCI (Molten Core Concrete Interaction) and/or over-pressurization of the containment. Core catcher channel is 0.1 m height and 16 m

* Communicating Author, School of Nuclear Engineering, Purdue University, West Lafayette, In 47906

width of large gap including 10° inclined channel and following vertical channel section. Top plate of the channel supplies decay heat generated from molten corium to liquid coolant and two-phase flow is generated with boiling.

To access safety performance of the core catcher system, it is essential to understand the two-phase flow behavior and flow structure as well as local void fraction distribution inside of the loop. However, since core catcher loop consists of a hydraulic diameter 20 cm of large channel, prediction two-phase flow structure inside of the channel using normal models developed on small diameter channels has a limitation. In addition, due to its geometrical complexity, experimental observation of two-phase characteristic is necessary. In a large diameter channel, channel size is larger than maximum bubble size and therefore large bubble breaks into two or more daughter bubbles because of surface instability [1]. There have been limited researches on two-phase flow in large diameter channel, and most of them are in vertical or horizontal flows. Lucas et al. [2] studied the air-water flows in a vertical large pipe with inner diameter of 19.53cm. They established accurate database on the two-phase flow for a wide range of flow rates. This database includes detailed information on the evolution of the flow along the large diameter vertical pipe. Oddie et al. [3] conducted the experiments of water-gas, oil-water and oil-water-gas multiphase flow on a transparent 11 m length and 15 cm diameter pipe. In this experiment, the pipe inclination was varied from 0° to 92°. The author studied the effects of the flow rates of different phases and pipe inclination on holdup and generated detailed flow pattern maps over a wide range of flow rates and pipe inclination. Although such database has been constructed on two-phase flow in different conditions, it still has difficulties on predicting two-phase flow in core catcher system, because of the geometrical uniqueness of core catcher loop which includes 10° inclined to vertical elbow bend. Bent large diameter pipes are commonly used in the reactor system. Therefore, more comprehensive researches of two-phase flow characteristics in such channel are required.

For these reasons, core catcher model facility is constructed with real scale except width using 30 cm instead of 16 m. The scaling analysis results are documented in detail in the paper by Revankar et al. [4].
In this study, air is generated by compressor instead of using steam. The purpose of the experiments is specialized in observing the two-phase flow dynamics. Flow development along the channel is visualized by high speed camera. Local void fraction is measured at several certain locations to analyze flow characteristics. The experimental data presented in this study provide the information of two-phase flow structure which can be applied not only to the core catcher channel but also to similar geometries including bended large diameter pipes in reactor system. Moreover, experimental results can validate and qualify the models for two-phase flow development and bubble breakup at the bend.

2. DESCRIPTION OF EXPERIMENTS

2.1. Modeled Flow Loop

Natural circulation flow loop is designed by scaling analysis through transient form of mass, momentum and energy balance equations [5]. Key integral scaling parameters are obtained by non-dimensionalization of the response functions. Channel height and length of the modeled facility along the flow direction is same as the prototype, but width is scaled down to 0.3 m instead of 16 m as in prototype. The area of test channel cross section is 0.3 m × 0.1 m which is channel width of 30cm and channel height of 10 cm. Diameter of down-comer pipe is determined by natural circulation flow rate balancing between hydrostatic pressure and frictional pressure drop. The determined size of down-comer in model facility is 4 inches(101.6 mm). Figure 1 shows the schematic of flow loop of modeled experimental facility constructed in POSTECH.

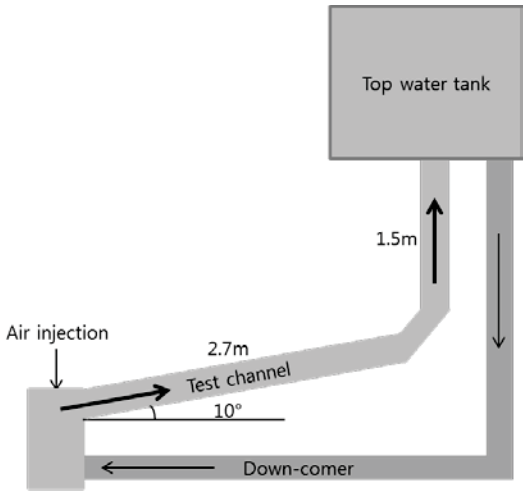

Figure 1. Schematic of experimental loop

Experimental facility consists of test channel, top water tank and down-comer. Air controlled by rotameter is injected perpendicular to the flow direction at 0.3 m horizontal test channel. Two-phase flow is developed along the flow test loop from 2.7 m inclined channel to 1.5 m vertical channel. Vertical channel includes flexible tube which connects between rectangular channel and top water tank. Air phase is separated from water at 1.2 m height of top water tank, and only water flows back to down-comer which makes natural circulation. Natural circulation flow rate is measured by paddle flow meter at down-comer horizontal part.

Whole test section including horizontal, inclined and vertical channel is made of polycarbonate plate to observe inside two-phase flow behavior. Since gas phase in the down-comer could disturb paddle flow meter measurement, top water tank is transparent to see if air flows back into down-comer pipe. In addition, transparent tube places before paddle flow meter to confirm no air is re-circulated.

2.2. Experimental Instrumentation

The instrumentations and control systems used in the experiments include:

- Rotameter – *Dwyer's RMC-106-SSV* is used to control supplied air flow rate. Measurable range is 50 to 500 L/min, and the accuracy is 2 % of full-scale.
- Paddle flow meter – *OMEGA's FP-5300* mounted on the horizontal part of down-comer measures natural circulation water flow rate. *OMEGA's FP-90* transmitter receives the signal from flow meter and averages it within 50 seconds. The range of flow meter is 0.3 to 6 m/s. Error of flow meter and transmitter are $\pm$1 % and 0.5 % respectively.
- Conductivity probes – Conductivity probes are made using diameter of 0.203 mm Pt/Rh alloy Tip. It is able to be mounted on the top wall. PTFE ferrule allows probes to move up and down. Void fraction is calculated by the voltage signal which probe supplies.
- DAQ, PC based data acquisition hardware *Measurement Computing's PCI-DAS6071* is used with sampling rate of 20 kHz.
- Video, High speed camera records in 3.8 seconds with 1000 frame per second.

2.3. Experimental Procedure

At the beginning of the experiment, probes are mounted on each location and inserted at a specific depth. Probes can be inserted into the channel from the top surface by using plastic ferrule compression fitting. After fixing the probes, water is filled up to 0.5 meter higher than down-comer inlet in order to avoid bubbles to enter the down-comer and/or the eruption of water from the top water tank. Air compressor is turned on and supplies the air into the horizontal channel from the top. By monitoring the probe signals, we adjust the threshold voltage of each probe. When threshold voltage is fixed properly, probe voltage signal varies distinguishing between water and gas phases. Once probe test is completed, certain amount of water is supplied in a few seconds until it becomes steady-states. Steady state is accomplished by checking the 50 seconds-averaged water flow rate. We consider the condition which is the averaged water flow rate not fluctuating ± 1 gallon per minute(3.8 liter per minute) as a steady state. Once the steady state is completed, data acquisition is started within 40 seconds. After the end of the data acquisition, signal of probe voltage and 50 seconds-averaged void fraction are saved. Once one air flow rate condition is finished, next air flow rate is set to be steady state. After one set of experiments including five air flow rate conditions are finished, we stop the air injection and change the probe positions from the top plate. The experiment of next set is continued with same procedure.

2.4. Experimental Matrix

The general purpose of the experiment is to observe the two-phase behavior through the elbow bend. Hence, more probes are mounted on elbow bend. Six locations shown in Figure 2 are selected to measure the void fraction inside of the flow loop.

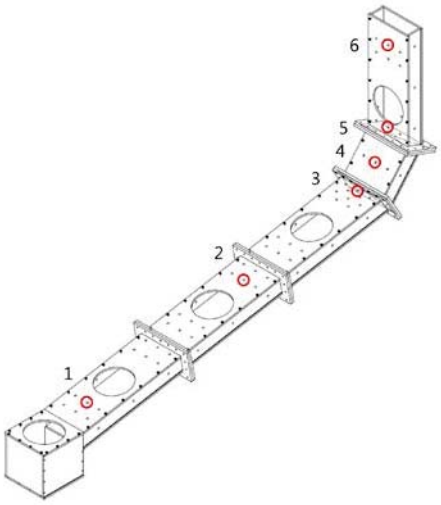

Figure 2. Measuring locations

Channel has 10 cm height and 30 cm width of rectangular shape which hydraulic diameter is 15 cm. Table 1 lists the distances between the inlet of inclined section and each measuring locations along the flow path.

Since prototype has 16 meter of channel width, lateral differences caused by side wall effect are not of interested in this experiment. Therefore, probes are mounted only on the center of the channel. Each location is measured at several heights from the top plate by inserting probes to obtain local profile of channel height direction. These inserting depths of probes and L/D of each location are shown in Table I. In this experiments, probe inserting depth and/or depth means probe tip distance from the top surface, while L means length from the inlet of inclined section to the measuring location. At location 1, no measurement has been conducted at the distance far from the top surface, because almost no bubbles are

detected there. Since no more than five probes can be measured at once due to the limitation of cables in the control box, two and four probes are measured separately. Each L and H is control box names and each control box operates eight sets of experiments. Totally 16 sets of experiments are conducted, and each includes 5 air flow rate cases.

Table I. Experimental matrix: Marked positions are measured.

Air flow rate Qg at each position: 100, 200, 300, 400, 500 L/min											
Location	L/D	0.5cm	1cm	1.5cm	2cm	3cm	4cm	5cm	7cm	9cm	9.5cm
1	1.3	L1	L2	L3	L4	L5	L6				
2	10.3	L1	L2	L3	L4	L5	L6	L7	L8		
3	16.8	H1	H2	H3	H4	H5		H6	H7	H8	
4	18.0	H1	H2	H3	H4	H5		H6	H7	H8	
5	19.4	H1	H2	H3	H4	H5		H6	H7	H8	
6	23.4	H1	H2		H3	H4		H5	H6	H7	H8

Each combination of air flow rate from 100 to 500 L/min is repeated 16 times by changing probe positions. Natural circulation flow rate measured by paddle flow meter at horizontal part of down-comer is an averaged value of 16 sets of experiments in each air flow condition. Table II provides 16 times averaged natural circulation water flow rate at each case.

Table II. Natural circulation flow rate

Air flow rate (L/min)	100	200	300	400	500
Superficial velocity of gas (m/s)	0.056	0.111	0.167	0.222	0.278
Water flow rate (L/min)	315	394	461	509	547
Superficial velocity of water (m/s)	0.175	0.219	0.256	0.283	0.304
Mass flux of water (kg/m^2sec)	668	835	978	1079	1162

Single phase natural circulation flow rate is obtained by supplied air flow rate. The maximum difference between 16 times measurements is 5.9% of average value.

3. RESULTS

3.1. Flow Visualization

High speed camera records in 3.8 seconds with 1000 frame per second. Figure 3 to 5 shows the visualized images when the air phase passes the screen. In the figure title, each time written in second indicates the time interval from 0 sec in each location.Two-phase flow structure is visualized by high speed camera along the flow channel from inclined to vertical through transparent polycarbonate plate. Since the experimental facility has unique and complex geometry, it is difficult to predict inside two-phase behavior. Therefore observing inside of the flow channel could give an insight into how two-phase flow behaves in a large channel natural circulation loop. Also high speed camera view helps to understand the physics and mechanism of bubble breakup and coalescence.

In figure 2, location 1 and 2 are located at inclined channel. Location 3, 4 and 5 are located just before, in the middle and just after the elbow bend, while location 6 is at vertical channel. In every location, flow is visualized at 100 L/min gas injection flow rate.

Figure 3 presents flow pattern along the inclined section. Each figure shows 10° inclined channel with 10 cm height with flowing from the lower left to the upper right. The dark shadow at the upper surface is air phase while the bright color shows liquid phase.

At location 1, air moves alongside to top wall. Top surface of the channel is dried for a long time because very long elongated bubbles or slugs flow with contacting to top wall. Since figure (a) and (b) are the position located near the inlet which L/D is 1.3, it is possible to consider this flow condition as an inlet condition. Thin and long slug passing near the top wall becomes thicker and shorter by expanding air-phase to the lower height of channel. This thicker bubble makes vortices and waves behind it because of induced turbulent swirl. Therefore elongated bubble tail breaks into many small bubbles, and the broken small bubbles are distributed even the lower height of the channel. At location 2, flow pattern shows slug/churn flow with small bubbles detaching behind and moving downwards the channel

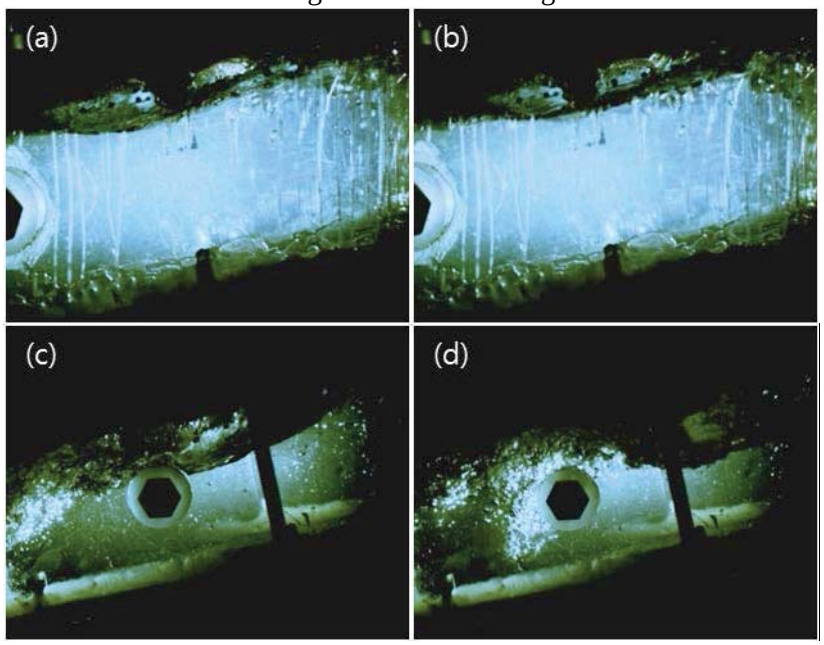

Figure 3. Flow pattern side view at Q_g=100 L/min
(a) location 1, 0 sec; (b) location 1, 0.1 sec; (c) location 2, 0 sec; (d) location 2, 0.1 sec

At location 3 and 4 in the figure 4, we can observe dynamic bubble behavior at the bend. In figure 4, (a) and (b) show the position near location 3 which is inclined channel just before the elbow bend. Length from location 3 probe to bending edge is 3 cm. Figure 4 (c), (d), (e) and (f) describe the flow pattern at elbow bend connecting between 10° inclined channel and vertical channel which has 50° inclination.

The slug size presented in figure 4 (a) and (b) increases in both height and width. Air phase coalesce to become a more stable size of slugs. Large size slug passes fast and water wets the surface for a long time. However this enlarged bubble cannot maintain its stability and undergo drastic changes when it flows into the elbow bend. Once the bubble nose enters the elbow bend, bubble is accelerated because of the larger effective buoyancy force. Air expands and fills the large area of the bend channel until bubble tail enters the bend. Figure 4 (c) shows the moment when the entire slug enters the channel. It breaks into lots of small bubbles with big swirl from the bubble tail because of water ingression into the bubble. In figure 4 (d), a slug is struck by a wave, and then it breaks with swirl shown in (e) and (d).

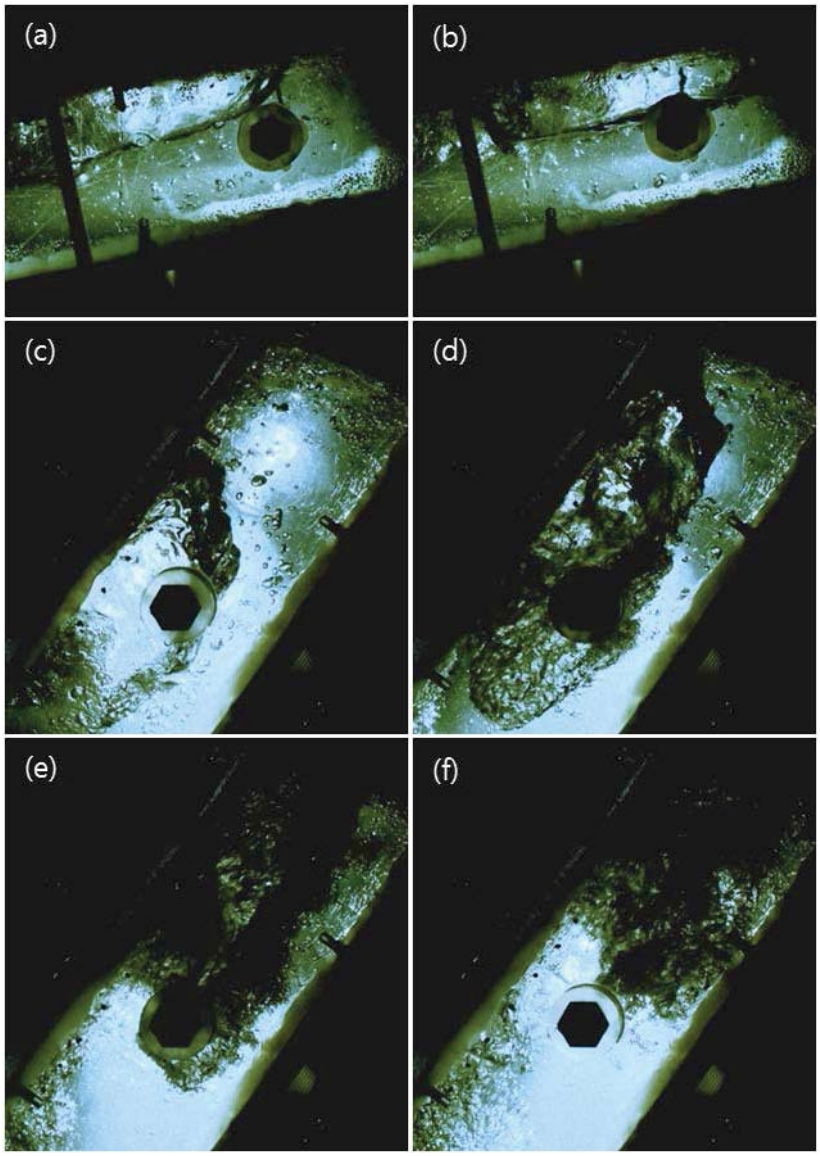

Figure 4. Flow pattern side view at Q_g=100 L/min
(a) location 3, 0 sec; (b) location 3, 0.1 sec;
(c) location 4, 0 sec; (d) location 4, 0.05 sec; (e) location 4, 0.1 sec; (f) location 4, 0.15 sec

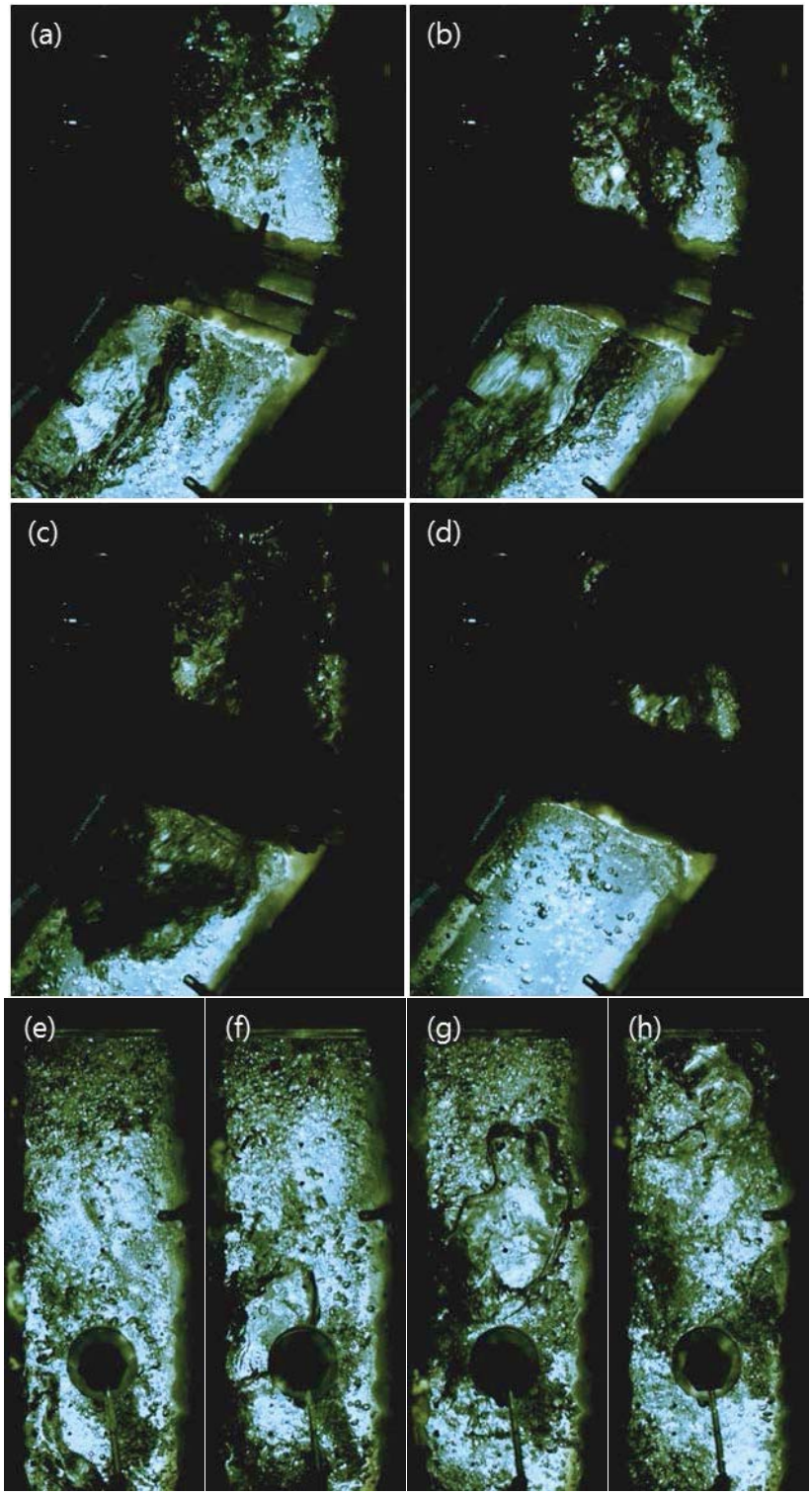

Figure 5. Flow pattern side view at Q_g=100 L/min
(a) location 4 to 5, 0 sec; (b) location 4 to 5, 0.05 sec;
(c) location 4 to 5, 0.1 sec; (d) location 4 to 5, 0.15 sec;
(e) location 5, 0 sec; (f) location 5, 0.05 sec; (g) location 5, 0.1 sec; (h) location 5, 0.15 sec

Figure 5 shows flow pattern after elbow bend. (a), (b), (c), and (d) show the flow between 50° bend to vertical channel, and (e), (f), (g), and (h) show the vertical upward flow. Bubble breakup occurs again between 50° bend to vertical channel with same mechanism. Most of the slugs become small bubbles while passing the elbow bend, while some of them still survive partially. They are again broken into pieces soon due to the high turbulence. Various size of bubbles exist in the figure 5 (e), (f), (g), and (h) where is just after the elbow bend. It is clear that flow pattern changes at the elbow bend. As a result, flow regime in higher part of vertical channel presents turbulent bubbly flow without big swirl.

3.2. Local Void Fraction

Local void fraction measured by conductivity probes is time-averaged value within 40 seconds. Local void fraction is not cross-sectional averaged spatial value, but time averaged value at specific location. Local void fraction is defined as a ratio of time for probe tip being surrounded by air to total time.

3.2.1. Local void fraction distribution

Figure 6 shows time averaged local void fraction distribution along the flow path at various distances from the top plate. Understandably local void fraction normally increases as injected air flow rate increases from 100 L/min to 500 L/min. Even the absolute value of local void fraction increases, but the trend shows almost same in various air injection flow rate. Therefore, it is considered that the mechanism which makes this characteristic is similar in various air inlet conditions.

Local void fraction at 0.5 cm and 1 cm distance from top wall generally decreases through the flow path. The local void fraction decreases abruptly at the elbow bend (location 3 to location 5). Higher local void fraction at upward (location 1 and 2) means air phase stays more time on that position. That is, air phase near the top wall stays longer at lower L/D in inclined channel. On the other hand, water wets the top surface longer time at higher L/D in inclined channel. This trend seems reasonable when comparing with figure 3 and 4. Probe inserting depth changes from 2 cm to 3 cm, the overall graph trend becomes flat. In 5 cm depth, inclination of the graph reverses which means local void fraction of higher location is higher than that of lower location. In inclined channel, local void fraction at inserting depth 5, 7 and 9 cm is very low because elongated bubbles near the top are not extended to the lower part of the channel. However at location 2, gas phase is detected even at the lower part, because small bubbles come away from elongated bubble tail and passes lower part of the channel slowly. However probe at location 3 detects almost no air in 5 cm depth since small bubbles move fast near the top wall following slugs. The graph at 5 and 7 cm 9 shows similar trend.

3.2.2. Local void fraction profile at each location

The figure 7 shows the local void fraction at each location measured in various depths. Horizontal axis is the distance from top surface which means the probe inserting depth. Dimensionless depth 0 presents the top wall while 1.0 is the bottom of the 10 cm channel. It is possible to define that location 1 as an inlet condition because it is very close to the air inlet. Since air is supplied from the top surface and because of the buoyancy force, it is quite obvious that local void fraction is higher near top surface. Local void fraction profile at inclined section including location 1, 2 and 3 has similar trends that local void fraction is high near the top surface and get lower near the bottom of the channel. But the inclination of the graph decreases from location 1 to location 3. It stands for that air phase distributes broadly in the channel as the flow develops. This kind of trend suddenly changes at location 4 and 5. While large bubbles passing this transition section, bubble breakup occurs in very turbulent way. Through bubble breakup process at the elbow bend, more air is detected at the lower part of the bend. A remarkable result is that local void fraction near top wall is very low because of water ingression into the slug touching top wall of the

channel. This striking wave wets the top surface of the channel, so top wall is normally not in a dry condition. It is desirable to increase the local heat transfer coefficient, which makes the core catcher system more efficient in cooling the molten core. At location 6, where the downstream of the vertical channel, void fraction spreads more evenly in depth direction. Lots of small bubbles flow in very turbulent way which makes a nearly flatter void fraction profile.

3.3. Center Line Averaged Void Fraction

Center line averaged void fraction is an averaged void fraction calculated by integrating local void fraction profile along the channel height. For example, center line averaged void fraction at location 4 is the area surrounded by red line and horizontal axis in Figure 7 graphs. The void fraction at the position very close to the wall is obtained by linear extrapolation. Figure 8 shows center line averaged void fraction along the flow path. In the figure 8, particularly low averaged void fraction is seen at the elbow bend. Lower height averaged void fraction means higher gas velocity in the channel. This trend is attributed to the bubble acceleration at the bend. Just before and after the bend (location 3 and 5) indicates similar low line averaged void fraction due to the effect of elbow bend. Bubble breakup by water ingression starts at location 3, and some survived slug still experiences bubble breakup at location 5. At location 6, void fraction increases again and shows highest value. Small bubbles generated by passing through the elbow bend move in very turbulent way. They create the large swirl of bubbles and reverse current at the vertical channel and thereby recirculation occurs. So the highest averaged void fraction is measured at location 6. The more air is supplied, the higher averaged void fraction is appeared. In all kinds of air flow rate condition, the graph shows similar trend that averaged void fraction decreases at the bend and increases again at the vertical channel. However, as the air flow rate increases, more pronounced tendency is observed, because in higher air flow rate condition bubble breakup occurs more actively due to high turbulence.

4. CONCLUSIONS

Since passively actuating core catcher cooling loop is composed of large channel with unique geometry, experimental study has been required to predict flow structure inside of the channel. Flow structure is visualized along the loop by high speed camera. Sudden change of flow structure is produced passing through the elbow bend because of bubble breakup caused by water ingression. Elongated bubbly or slug/churn flow is shown in inclined channel, while turbulent bubbly flow is observed at vertical channel. This flow structure transition is quantitatively analyzed by using local void fraction data. The graphs clearly show a sudden change of local void fraction distribution. Low local void fraction near top wall is desirable to increase the local heat transfer coefficient, which makes the core catcher system cool the molten core more efficiently. Local void fraction at each location is integrated along the depth of channel. This center line averaged void fraction suggests flow acceleration at elbow bend and recirculation at vertical channel. The void fraction distribution and profile analysis is carried out to understand flow structure in the core catcher cooling channel.

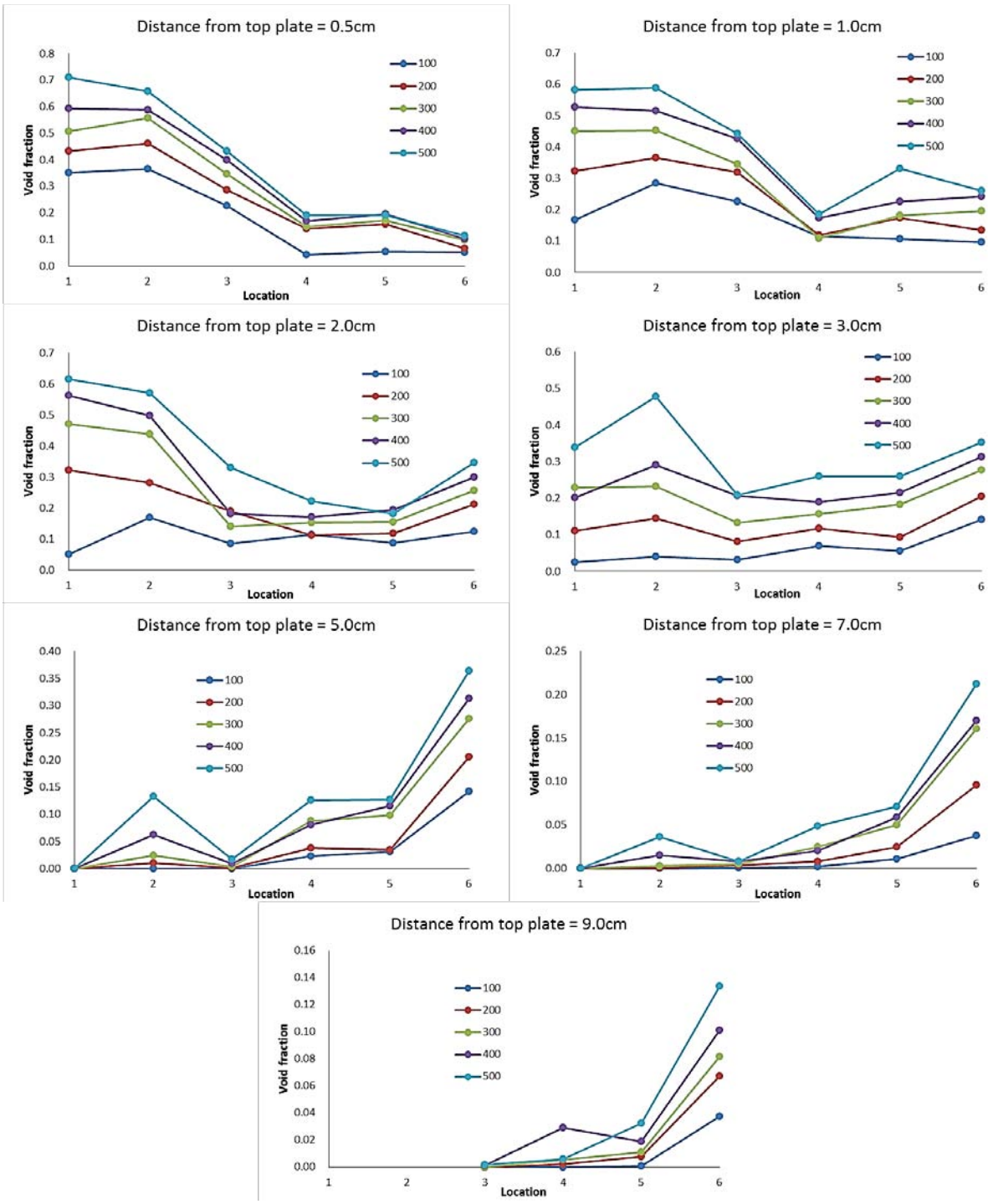

Figure 6. Local void fraction along the flow path

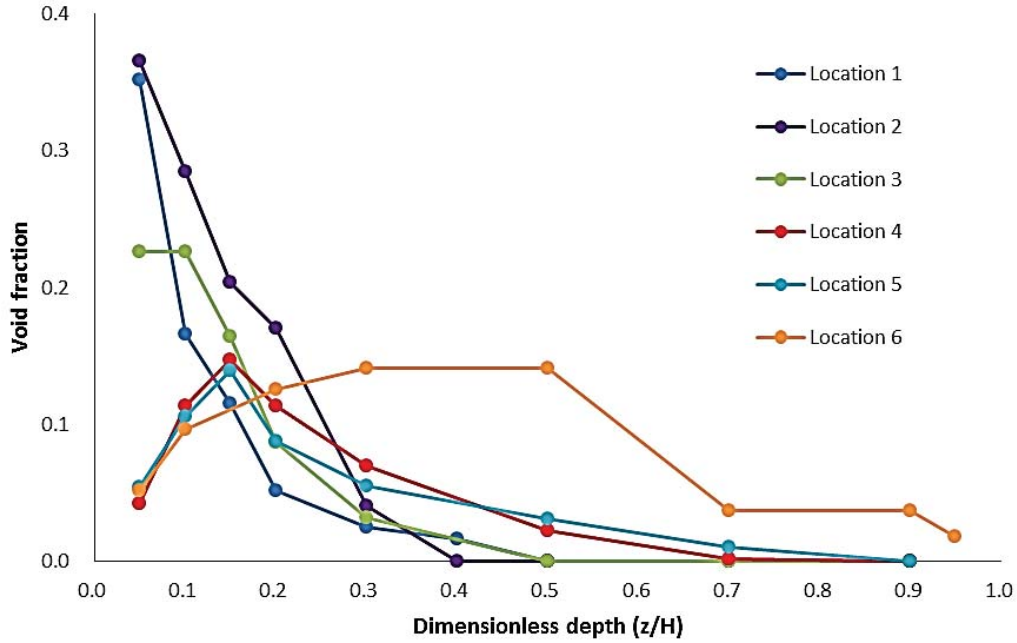

Figure 7. Local void fraction profile at each location at Q_g=100 L/min

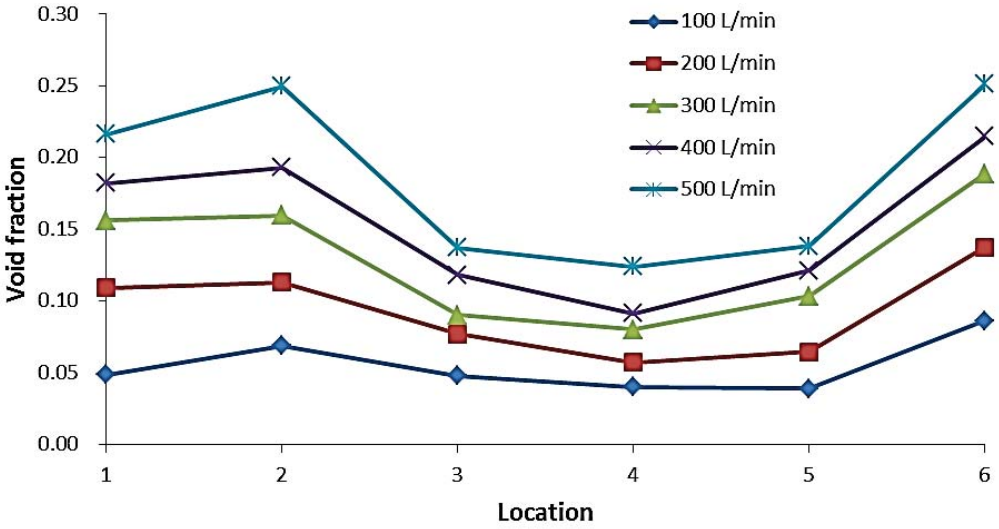

Figure 8. Center line averaged void fraction along the flow path

ACKNOWLEDGMENTS

The work is supported by the Korea Atomic Energy Research Institute (KAERI).

REFERENCES

1. Batchelor, G. K. "The stability of a large gas bubble rising through liquid." Journal of Fluid Mechanics 184 (1987): 399-422.
2. Lucas, D., et al. "A new database on the evolution of air-water flows along a large vertical pipe." International Journal of Thermal Sciences 49.4 (2010): 664-674.
3. Oddie, G., et al. "Experimental study of two and three phase flows in large diameter inclined pipes." International Journal of Multiphase Flow 29.4 (2003): 527-558.
4. Revankar, S. T., et al. "Simulation of two-phase natural circulation cooling using air water system." Procedia Engineering 56 (2013): 126-133.
5. Ishii, M., et al. "The three-level scaling approach with application to the Purdue University Multi-Dimensional Integral Test Assembly (PUMA)." Nuclear Engineering and Design 186.1 (1998): 177-211.